Scientific Papers. Series E. Land Reclamation, Earth Observation & Surveying, Environmental Engineering. Vol. XV, 2026
Print ISSN 2285-6064, CD-ROM ISSN 2285-6072, Online ISSN 2393-5138, ISSN-L 2285-6064

COMPARATIVE ANALYSIS OF ALTIMETRIC VARIATIONS IN THE SLĂNIC PRAHOVA AREA BASED ON LEVELING MEASUREMENTS

Mihai AVADANEI[1, 2], Tiberiu POPESCU[2], Florina ȚERLE BURESCU[1], Florin SALA[3, 4], Mihai Valentin HERBEI[1, 3]

[1]University of Petrosani, 20 University Street, 332006, Petroșani, Romania
[2]S.C. Top Geocart S.R.L., 67 Prof. I. Marinescu, 021244, District 2, Bucharest, Romania
[3]University of Life Sciences "King Mihai I" from Timisoara, 119 Calea Aradului, 300645, Timisoara, Romania
[4]Agricultural Research and Development Station Lovrin, 307250, Lovrin, Timis, Romania

Corresponding author email: florin_sala@usvt.ro

Abstract

The levelling measurement campaign carried out in Slănic Prahova, Prahova County, year 2025, aimed to monitor altitude variations in the locality urban area. The measurements were performed with a high-precision Leica LS15 instrument and differential compensation methods, using the national E-TransDatRO system and the EGG97&MN75 geoid model. The route included locations between stations, with double observations, over length of over 2.19 km. The comparison of the two campaigns suggested a minimal evolution of the topographic surface, within the limits of the instrumental tolerances. The results obtained indicated a very good closure of the networks, with insignificant differences, which confirmed the quality of the observation and the general stability of the terrain during the analysed interval. The configuration of the altimetric in profile highlighted areas of maximum in the centre of the route and progressive decreases towards the extremities, consistent with the local relief and the structure of the salt massif.

Key words*: altimetric profile, altitude variation, monitoring, subsidence, topographic surface.*

INTRODUCTION

Monitoring deformations associated with underground mining operations represents a major research direction in the field of engineering geodesy and rock mechanics, having direct implications for geotechnical risk assessment and surface infrastructure protection. The theoretical foundations of the behaviour of rock masses around underground excavations have been developed in classic works on rock mechanics, which highlight stress redistribution and progressive failure mechanisms (Hoek & Brown, 1980; Brady & Brown, 2006).

In the case of rock salt deposits, the mechanical behaviour is dominated by the rheological properties of halite, characterized by time-dependent creep, ductile deformation, and sensitivity to temperature and humidity conditions (Carter & Heard, 1970; Cristescu, 1989). The progressive deformation of the salt causes slow changes in the stress field, which can lead to differential settlements at the surface, even in the absence of sudden rupture phenomena (Bérest & Brouard, 2003). Constitutive models for rock salt have been developed to describe the visco-plastic behaviour of the massif and to allow predictive numerical simulations (Munson & Dawson, 1979). Similar studies have been done in areas with marble exploitation (Sîrbu et al., 2023).

In related research, the integration of numerical modelling with high-precision geodetic monitoring has become standard in the analysis of the stability of mining areas (Jing, 2003). Classical geometric levelling measurements remain the reference method for determining millimetre-scale altimetric variations (Ghilani & Wolf, 2012), while GNSS technologies allow the quantification of three-dimensional displacements and the stabilization of geodetic control networks. (Teunissen & Kleusberg, 1998; Cioflan et al., 2025). GIS facilities have been used for documentation in cadastral studies and territorial planning (Sîrbu et al., 2022; Tereşneu & Tereşneu, 2023).

A major development in deformation monitoring was the introduction of satellite-

based radar interferometry (InSAR), which allows the detection of millimeter-scale displacements over large areas (Massonnet & Feigl, 1998). The Persistent Scatterer InSAR method has significantly improved the accuracy and stability of displacement time series (Ferretti et al., 2001), and applications of this technology in mining areas have demonstrated its ability to identify slow subsidence and regional differential movements (Colesanti & Wasowski, 2006).

In addition, terrestrial laser scanning (TLS) and aerial scanning have allowed the generation of high-resolution digital surface models, useful for volumetric analysis and for detecting subtle morphological changes (Vosselman & Maas, 2010). The integration of data from GNSS, leveling and TLS into a unitary system leads to the development of 4D geospatial models (X, Y, Z, T), capable of describing the temporal evolution of the terrain (Lindenbergh & Pfeifer, 2005; Cioflan et al., 2025).

In parallel with the development of acquisition technologies, multivariate statistical methods have become essential tools in deformation analysis. Principal component analysis (PCA) allows reducing the dimensionality of large data sets and highlighting the dominant variables in the deformation process (Jolliffe, 2002). Cluster analysis techniques are also used to identify groups of landmarks with similar behaviour and to delimit areas with pronounced instability (Kaufman & Rousseeuw, 1990).

The Digital Twin concept, applied to infrastructures and the built environment, represents an advanced stage in predictive monitoring, through the real-time integration of data from multiple sensors and the continuous updating of the digital model of the site (Grieves & Vickers, 2017). This approach allows the transition from reactive to proactive monitoring, based on warning thresholds and forecasting models (Boje et al., 2020).

In the context of salt exploitation in Romania, the geological particularities of the salt regions and the history of large volumes of excavations require the use of integrated monitoring systems and rigorous data analysis methodologies (Săndulescu, 1984).

Correlating geodetic information with geomechanical modeling and hydrogeological parameters is essential for understanding deformation mechanisms and for substantiating technical decisions (Bell, 2007).

This scientific study aimed to analyze altimetric variations in the Slănic Prahova area in a modern research direction, which combined classical precision levelling methods with GNSS technologies and multivariate statistical analysis, in order to evaluate the differential behaviour of the terrain and the geotechnical risk associated with underground salt exploitation.

MATERIALS AND METHODS

General characterization of the study site area

The Slănic Prahova Salt Mine represents one of the oldest salt mines in Romania, its activity beginning in 1668 by exploiting the mines at "Băile Verzi", later followed by the opening of other mines. Initially, the extraction was carried out by digging large, trapezoidal-shaped chambers. In 1970, the mining process was modernized by introducing the method with small chambers and square pillars, arranged on superimposed horizons, first applied to the “Victoria” mine and, since 1992, to the “Cantacuzino” mine.

The rock salt deposit at Slănic Prahova has a lenticular shape, with a length of approx. 2,700 m, in the North-South direction, a width between 800 and 2300 m, and a maximum thickness of 499 m (Marina, 2023). The main types of rocks that appear within the deposit are: salt, volcanic tuffs, clays, marls and sandstones.

From a geographical point of view, the area falls within the hilly area of the “Curved Carpathians” mountains, with altitudes ranging between 359 m (in the “Slănic” stream valley) and 662.80 m (the “Gorganu” peak).

The relief is influenced by landslide processes, and the main collector of surface waters is the “Slănic” stream, which crosses the area above the deposit in the North–South direction, Figure 1.

The exploitation framework method adapted to the conditions of the deposit within the Cantacuzino mine, belonging to the Salina Slănic Prahova, is the "method with small rooms and abandoned square pillars, in the technological version with vaulted ceiling".

This technical solution was substantiated by the work entitled "Framework project of the rock

salt exploitation method with small rooms and abandoned (square) pillars, with vaulted ceilings", developed in 2002 by SC MINESA ICPM SA (Chipeșiu, 2015; Oprina, 2015).

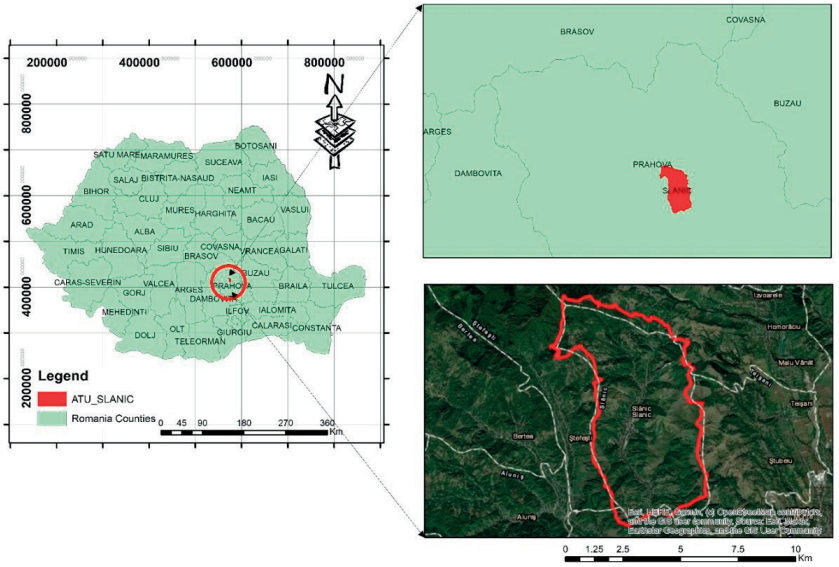


Figure 1. Map of the study area, Slanic ATU, Prahova County, Romania

Presentation of the study methodology

An advanced structural monitoring system has been implemented to study vertical and horizontal movements in the Slănic Prahova locality. The objective is to provide high-certainty data for risk assessment and to ensure the stability of critical infrastructure.

Ensuring structural stability in geologically risky areas, such as Slănic Prahova, requires a holistic approach and a complete synergy between ground and aerial measurement technologies. The objective of the study was to create a dynamic model (X, Y, Z, Time, Detail) for risk assessment.

To achieve the highest level of certainty, a monitoring workflow based on five technological pillars from Leica Geosystems was integrated:

• GNSS Monitoring: Establishes and maintains the fundamental geodetic network, controlling long-term horizontal displacements;

• Precision Leveling: Rigorously verifies structural settlements and elevations, providing the highest standard of Vertical Control;

• Leica MS60 MultiStation: Data fusion platform that delivers high-precision dynamic 3D measurements, monitoring subtle structural movements (Chen et al., 2023);

• Leica RTC360 Scanner: Provides fast, high-density 3D laser scanning, creating detailed Digital Twins of structures (Leica Geosystems, 2025a), Figure 2.



Figure 2. Leica MS60 multistation

• Leica BLK2fly (Autonomous Flying Scanner): Extends monitoring to the aerial level. We quickly capture data from above (facades, roofs, inaccessible or dangerous areas) and integrate the aerial point cloud with the terrestrial one to obtain a complete geometry of the site.

This convergence of sensors allows the transformation of raw data into predictive information, providing authorities with complete and rapid solutions for risk management and planning of consolidation works.

For the precision leveling works, the Leica LS15 digital level was used, a high-precision surveying instrument that offers an accuracy of up to 0.2 mm per double km of leveling, and automatic functions such as an integrated camera and autofocus that performs measurements on special barcoded stages. The Leica LS15 digital level is designed to increase efficiency and eliminate common human errors in demanding leveling tasks. The measurement method used was BF ("Back & Forth" leveling) and with the calculation of the average of 3 simultaneous measurements. The processing and compensation of the obtained data was done with the Leica Infinity software (Leica Geosystems, 2025b).

The monitoring of vertical and horizontal movements in the Slănic Prahova area was achieved by implementing an integrated structural monitoring system, based on the convergence of several geospatial technologies. The system was designed to generate a dynamic model of the type: $f(X, Y, Z, T)$, where: X, Y – planimetric coordinates; Z – altimetric coordinate; T – temporal coordinate.

For statistical data processing and generation of graphical representations, PAST software v. 4.17 (Hammer et al., 2001) and Mathematica software v. 14.2 (2024) were used.

RESULTS AND DISCUSSIONS

For each landmark common to the two measurement campaigns, the vertical displacement (ΔH) was determined by Equation (1) according to (Naumowicz & Kowalczyk, 2025), with the values presented in Table 1. Of the total number of markers installed in the area affected by the landslide in Slanic Prahova, only those located at ground level were analyzed (Table 1, Figure 3). The rest of the markers were placed on the affected buildings, and for them a separate monitoring was carried out, using the same method and the same equipment, the Leica LS15 digital level, for leveling measurements.

$$\Delta H = H_{nov} - H_{sep} \quad (1)$$

where: ΔH – elevation difference; H_{nov} – elevation in november; H_{sep} – elevation in september

Table 1. Benchmark values during the study period

Ground Repers	H_{sep}	H_{nov}	ΔH
	(m)		
R2	393.1642	393.1534	-0.0108
R3	394.5307	394.5421	0.0114
R11	396.6375	396.6751	0.0376
R12	395.3027	395.3462	0.0435
R13	394.5393	394.5775	0.0382
R14	394.5875	394.6382	0.0507
R15	395.4677	395.5223	0.0546
R16	427.0541	427.1344	0.0803
R17	419.0415	420.0313	0.9898
R19	414.0677	414.1524	0.0847
R20	413.5401	413.6251	0.085
R21	406.7232	406.8136	0.0904
R22	403.4683	403.5619	0.0936
R23	399.4444	399.5438	0.0994
R25	390.3181	390.4193	0.1012
R26	391.3027	391.4078	0.1051

The reference elevation that was used in both measurement sessions was located on a pillar that was in the area of influence of the collapse, so these recorded differences occurred due to the fact that the pillar underwent elevation movements. This was highlighted by post-processing GNSS data, both in September and November. Thus, it was observed that compared to the initial elevation, the landmark had a difference of 5 cm in minus, which also influenced the other elevations. Following this finding, the technical commission decided to expand the monitoring area and place pilasters outside the affected area.

Between the two monitoring campaigns, significant altimetric variations were recorded, with amplitudes ranging between -0.0108 m

and +0.1051 m, for most landmarks and approximately +0.9898 m in the case of landmark R17. The spatial distribution of the differences indicated a differential behaviour of the terrain, with the delimitation of a sector of accentuated instability. The high values determined for markers R16 – R26 suggested the existence of a progressive deformation process. Marker R17 marked an area with major instability, which requires continuous monitoring and detailed analysis. The pedological context of the analyzed area may constitute a factor favouring the manifestation of these processes.



Figure 3. Initial leveling in the locality of Slanic Prahova, according to altimetric profile

The ΔH distribution showed a progressive character, suggesting the existence of a deformation gradient in the direction of the alignment of the landmarks.

The almost monotonic increase indicated a systematic differential behaviour, not random variations.

Depending on the recorded values, a four-level classification was made: Level 1, ΔH<2 cm (stable); Level 2, ΔH = 2-6 cm (moderate); Level 3, ΔH = 6.20 cm (high); Level 4, ΔH>20 cm (critical). The distribution by risk classes highlights the existence of a critical sector (Level 4) associated with the R17 landmark, distinct from the general deformation background (Level 3), which confirms the localized nature of the major instability.

The displacement from the critical area is approximately 15 times greater than the average deformation background, indicating a severe local mechanism, different from the general behaviour of the terrain, with examples in Figure 4.



Figure 4. Aspects recorded in Slanic Prahova locality

For each data series, the average value was calculated, and the difference of each elevation from the average value. In the case of the September data series, the average value was $\overline{H_{sep}}$ = 401.820 m (Table 2). Compared to the mean value, four benchmarks were recorded with values above the mean, and statistically significant differences, p<0.001 (R16, R17,

R19, and R20), respectively eight benchmarks with values lower than the mean, and statistically significant differences at the $p<0.001$ level (R25), at the $p<0.01$ level (R2, R26), and at the $p<0.05$ level (R3, R12, R13, R14, R15). In the case of the other benchmarks, the differences did not present statistical certainty.

In the case of the November data series, the average value was $\overline{H_{nov}}$ = 401.950 m (Table 3).

Table 2. Differences and significance in the case of the September measurement campaign

Benchmark	Given mean	Sample mean	95% conf. interval	Difference	95% conf. interval	t	p (same mean)	Sig
R2	393.164	401.820	(395.92 407.72)	8.660	(2.7599 14.56)	3.1285	0.0069	oo
R3	394.531			7.294	(1.3934 13.194)	2.6348	0.0188	o
R11	396.638			5.187	(-0.71337 11.087)	1.8737	0.0806	ns
R12	395.303			6.522	(0.62143 12.422)	2.3559	0.0325	o
R13	394.539			7.285	(1.3848 13.185)	2.6317	0.0189	o
R14	394.588			7.237	(1.3366 13.137)	2.6143	0.0195	o
R15	395.468			6.357	(0.45643 12.257)	2.2963	0.0365	o
R16	427.054			25.230	(19.33 31.13)	-9.1142	1.67E-07	***
R17	419.042			17.217	(11.317 23.117)	-6.2197	1.64E-05	***
R19	414.068			12.243	(6.3431 18.144)	-4.4229	0.0005	***
R20	413.540			11.716	(5.8155 17.616)	-4.2323	0.0007	***
R21	406.723			4.899	(-1.0014 10.799)	-1.7697	0.0971	ns
R22	403.468			1.644	(-4.2563 7.5442)	-0.5939	0.5615	ns
R23	399.444			2.380	(-3.5203 8.2802)	0.8598	0.4035	ns
R25	390.318			11.506	(5.606 17.406)	4.1566	0.0008	ooo
R26	391.303			10.522	(4.6214 16.422)	3.8009	0.0017	oo

Table 3. Differences and significance in the case of the November measurement campaign

Benchmark	Given mean	Sample mean	95% conf. interval	Difference	95% conf. interval	t	p (same mean)	Sig
R2	393.153	401.950	(395.99 407.9)	8.793	(2.835 14.751)	3.1456	0.0067	oo
R3	394.542			7.404	(1.4463 13.363)	2.6488	0.0182	o
R11	396.675			5.271	(-0.68672 11.23)	1.8858	0.0788	ns
R12	395.346			6.600	(0.64218 12.558)	2.3612	0.0322	o
R13	394.578			7.369	(1.4109 13.327)	2.6362	0.0187	o
R14	394.638			7.308	(1.3502 13.266)	2.6145	0.0195	o
R15	395.522			6.424	(0.46608 12.382)	2.2982	0.0364	o
R16	427.134			25.188	(19.23 31.146)	-9.0106	1.93E-07	***
R17	420.031			18.085	(12.127 24.043)	-6.4696	1.06E-05	***
R19	414.152			12.206	(6.2477 18.164)	-4.3665	0.0006	***
R20	413.625			11.679	(5.7204 17.637)	-4.1779	0.0008	***
R21	406.814			4.867	(-1.0911 10.825)	-1.7411	0.1021	ns
R22	403.562			1.615	(-4.3428 7.5735)	-0.5779	0.5719	ns
R23	399.544			2.403	(-3.5554 8.3609)	0.8595	0.4036	ns
R25	390.419			11.527	(5.5691 17.485)	4.1237	0.0009	ooo
R26	391.408			10.539	(4.5806 16.497)	3.7701	0.0019	oo

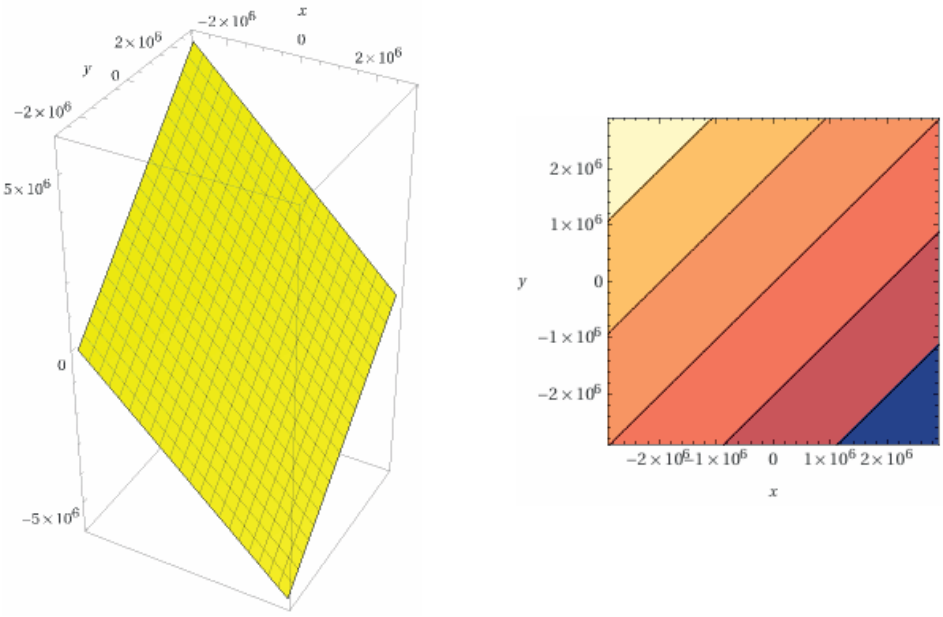
Compared to the mean value, four benchmarks were recorded with values above the mean, and statistically significant differences, $p<0.001$ (R16, R17, R19, and R20), respectively eight benchmarks with values lower than the mean, and statistically significant differences at the $p<0.001$ level (R25), at the $p<0.01$ level (R2, R26), and at the $p<0.05$ level (R3, R12, R13, R14, R15). In the case of the other benchmarks, the differences did not present statistical certainty.

Regression analysis was applied to find the

mathematical model that described the variation of ΔH in relation to the values of H_{sep} (variable x) and H_{nov} (variable y). The result was equation (2), with R^2 = 0.999, p<0.001, with the graphical representation in Figure 5.

$$\Delta H = a\,x^2 + b\,y^2 + c\,x + d\,y + e\,xy + f \quad (2)$$

where: ΔH – the difference in height of the landmarks between the two measurement campaigns; x – H_{sep} (m); y – H_{nov} (m); a, b, c, d, e, f – coefficients of Equation (2); a = -6.3E-13; b = -6E-13; c = -0.999999999990167; d = 0.999999999990152; e = 1.23E-12; f = 3.46E-12.



(a) (b)

Figure 5. Graphical representation of the variation ΔH in relation to H_{sep} (x axes) and H_{nov} (y axes)

According to the PCA analysis, the benchmark score values in relation to the Principal Components were obtained, Table 4. The highest values in PC1 and PC2 were recorded for benchmark R17, associated with which the largest deviation was recorded, as a result of the dip (H_{nov} compared to H_{sep}).

The multivariate analysis generated a PCA diagram (Figure 6), with the distribution of markers correlated with the two measurement campaigns (PC1 = 77.251%, and PC2 = 22.479%, of total variance).

The positioning of marker R17 correlated with ΔH was observed, a marker that stood out with the highest level of deviation between the two measurement dates.

Associated with H_{sep}, H_{nov} (as biplot) the markers R16, R19, R20, R21 and R22 were positioned.

Table 4. Benchmark score in the Principal Components

Benchmark	PC 1	PC 2	PC 3
R2	-1.2462	-0.0168	-1.93E-15
R3	-1.0472	-0.0095	-1.81E-15
R11	-0.7561	-0.0288	-2.75E-15
R12	-0.8965	0.0690	-2.61E-15
R13	-0.9938	0.0920	-3.86E-16
R14	-0.9639	0.1368	-3.42E-15
R15	-0.8560	0.1019	-2.47E-15
R16	2.7911	-1.5837	-2.79E-15
R17	3.6577	2.3278	-2.33E-15
R19	1.3209	-0.8338	-1.91E-15
R20	1.2614	-0.8029	-8.89E-16
R21	0.4957	-0.3974	-1.74E-15
R22	0.1313	-0.2015	-1.41E-15
R23	-0.3156	0.0478	-2.97E-15
R25	-1.3513	0.5699	-3.61E-15
R26	-1.2315	0.5291	-2.72E-15

The other markers were positioned independently of the factors H_{sep}, H_{nov}, ΔH, as biplots in the PCA analysis.

The cluster analysis (two-way) generated the dendrogram of association of the landmarks based on similarity (Coph.corr. = 0.880) in relation to the H (m) values, Figure 7. In the case of landmark R17, delimitation was observed based on the H (m) values in relation to the two measurement campaigns, H_{sep}, and H_{nov}.

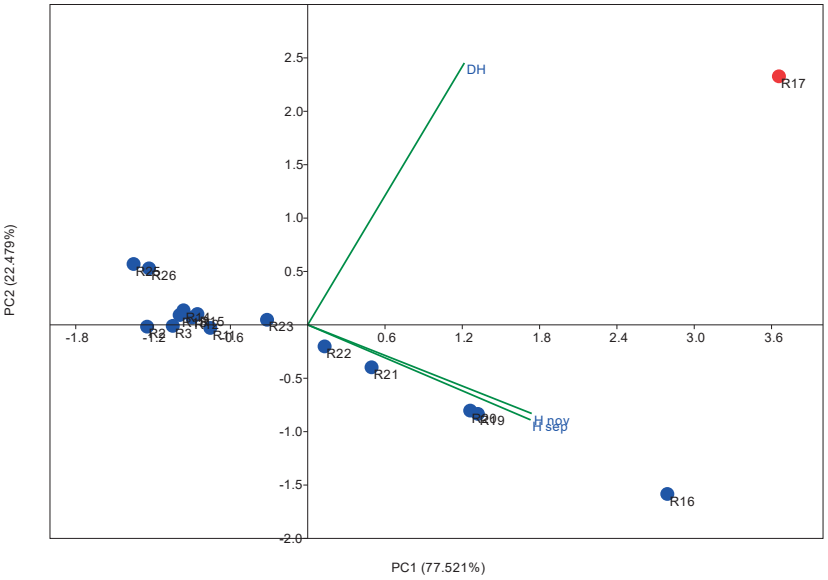


Figure 6. PCA diagram

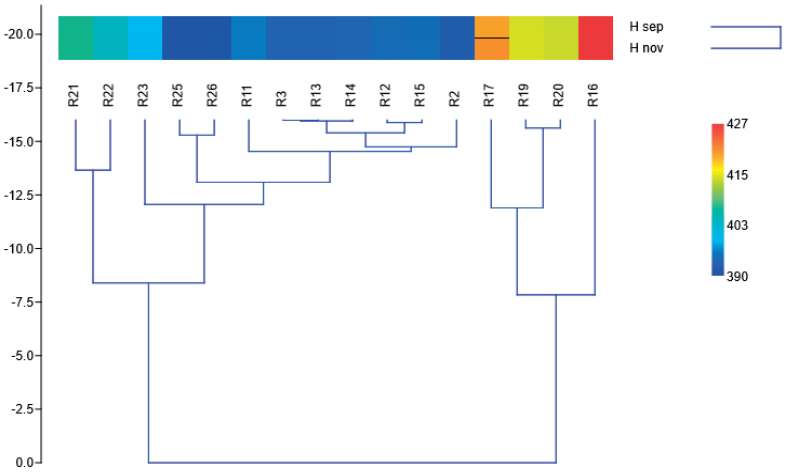


Figure 7. Cluster dendrogram of landmark association based on similarity

SDI (Similarity and Distance Indices) values were determined for the measurement reference points, Table 5. Low values indicate high levels of similarity, and high values indicate large differences between reference points.

Table 5. SDI values for the considered landmarks, in relation to the differences recorded

	R2	R3	R11	R12	R13	R14	R15	R16	R17	R19	R20	R21	R22	R23	R25	R26
R2		1.949	4.946	3.063	1.980	2.057	3.305	47.992	37.311	29.630	28.884	19.248	14.646	8.960	3.947	2.551
R3	1.949		2.998	1.115	0.036	0.111	1.356	46.043	35.362	27.681	26.935	17.299	12.698	7.011	5.895	4.499
R11	4.946	2.998		1.883	2.967	2.890	1.642	43.046	32.365	24.684	23.938	14.301	9.700	4.014	8.892	7.496
R12	3.063	1.115	1.883		1.084	1.007	0.241	44.929	34.247	26.567	25.821	16.184	11.583	5.897	7.009	5.613
R13	1.980	0.036	2.967	1.084		0.078	1.325	46.013	35.331	27.651	26.905	17.268	12.667	6.981	5.925	4.529
R14	2.057	0.111	2.890	1.007	0.078		1.248	45.936	35.254	27.574	26.828	17.191	12.590	6.904	6.002	4.606
R15	3.305	1.356	1.642	0.241	1.325	1.248		44.688	34.006	26.326	25.580	15.943	11.342	5.656	7.250	5.854
R16	47.992	46.043	43.046	44.929	46.013	45.936	44.688		10.707	18.362	19.108	28.745	33.346	39.032	51.938	50.542
R17	37.311	35.362	32.365	34.247	35.331	35.254	34.006	10.707		7.701	8.445	18.068	22.667	28.351	41.255	39.859
R19	29.630	27.681	24.684	26.567	27.651	27.574	26.326	18.362	7.701		0.746	10.382	14.984	20.670	33.576	32.180
R20	28.884	26.935	23.938	25.821	26.905	26.828	25.580	19.108	8.445	0.746		9.637	14.238	19.924	32.830	31.434
R21	19.248	17.299	14.301	16.184	17.268	17.191	15.943	28.745	18.068	10.382	9.637		4.601	10.288	23.193	21.797
R22	14.646	12.698	9.700	11.583	12.667	12.590	11.342	33.346	22.667	14.984	14.238	4.601		5.687	18.592	17.196
R23	8.960	7.011	4.014	5.897	6.981	6.904	5.656	39.032	28.351	20.670	19.924	10.288	5.687		12.905	11.510
R25	3.947	5.895	8.892	7.009	5.925	6.002	7.250	51.938	41.255	33.576	32.830	23.193	18.592	12.905		1.396
R26	2.551	4.499	7.496	5.613	4.529	4.606	5.854	50.542	39.859	32.180	31.434	21.797	17.196	11.510	1.396	

From the correlated analysis of the four risk levels with the grouping based on the similarity of the landmarks (Figure 5), the landmarks were associated with the sinking risk classes: Level 1, $\Delta H<2$ cm (stable) – R2, R3; Level 2, $\Delta H = 2 – 6$ cm (moderate) – R11, R12, R13, R14, R15; Level 3, $\Delta H = 6 - 20$ cm (high) – R16, R17, R19,R20, R21, R22, R23, R26; Level 4, $\Delta H>20$ cm (critical) – R17.

CONCLUSIONS

Through the evaluation method (BF) and the precision technique used, the study facilitated the obtaining of important information regarding the condition of the land in the Slanic Prahova locality, in relation to the recorded subsidence phenomenon.

The 16 landmarks (R2 to R26), placed on the ground in representative locations, indicated the changes in height (H, m) of the terrain, during the measurement campaigns between September and November, 2025. Based on the recorded values (H_{sep}, H_{nov}) the ΔH values were calculated, which highlighted the differentiated behavior of the terrain. With high changes, the landmark R17 was highlighted, with ΔH = 0.096 m.

Quadratic regression analysis generated mathematical and graphical models that described the variation in ΔH in relation to the variables x (H_{sep}) and y (H_{nov}) in conditions of statistical safety ($p<0.001$). Multivariate analysis (PCA) described the correlation of the benchmarks with the factors (H_{sep}, H_{nov}, ΔH), generated the score values of the benchmarks in relation to the Principal Components, within which the benchmark R17 was highlighted with the highest values in PC1 and PC2. Cluster analysis facilitated the grouping of landmarks based on similarity in relation to the H (m) values from the two measurement campaigns (H_{sep}, H_{nov}) and highlighted the differences recorded by landmark R17.

Based on the recorded values (ΔH), four risk levels for the sinking phenomenon were identified, Level 1, $\Delta H<2$ cm (stable); Level 2, ΔH = 2-6 cm (moderate); Level 3, ΔH = 6.20 cm (high); Level 4, $\Delta H>20$ cm (critical).

The results already recorded are important for local authorities in management decisions for the Slanic Prahova locality, in relation to risk levels, and further monitoring of the benchmark values will complete the database and update the situation in the field.

ACKNOWLEDGMENTS

The authors thank the GEOMATICS Research Laboratory, ULS "King Mihai I" from Timisoara, for the facility of the software used for this study. The authors also thank the company Top Geocart SRL for providing access to the equipment and software necessary for the preparation of this paper.

REFERENCES

Bell, F. G. (2007). *Engineering Geology*. 2nd Edition Butterworth-Heinemann, pp. 592.

Bérest, P., & Brouard, B. (2003). Safety of salt caverns used for underground storage. *Oil & Gas Science and Technology, 58*(2), 361–384.

Boje, C., Guerriero, A., Kubicki, S., & Rezgui, Y. (2020). Towards a semantic Construction Digital Twin. *Automation in Construction, 114*, 103179.

Brady, B. H. G., & Brown, E. T. (2006). *Rock Mechanics for Underground Mining.* Springer, pp 628.

Carter, N. L., & Heard, H. C. (1970). Temperature and rate-dependent deformation of halite. *American Journal of Science, 269*, 193–249.

Chen, Z., Shao, F., Fan, Z., Wang, X., Dong, C., Dong, Z., Fan, R., & Chen, D. (2023). A calibration method for time dimension and space dimension of streak tube imaging Lidar. *Applied Sciences, 13*(18), 10042.

Chipeşiu, F. (2015). *Optimizarea metodelor de exploatare la extragerea în stare solidă a zăcămintelor de sare gemă din România* [Optimization of mining methods for the solid-state extraction of rock salt deposits in Romania] [Doctoral dissertation, University of Petroşani].

Cioflan, F. M., Irimie, F., & Sabau, N. C. (2025). Technical methodologies for cadastral plan development using GNSS and UAV technologies: A case study in Pietroasa, Romania. *Scientific Papers. Series E. Land Reclamation, Earth Observation & Surveying, Environmental Engineering, XIV*, 827–838.

Cristescu, N. D. (1989). *Rock Rheology*. Springer, pp. 336.

Colesanti, C., & Wasowski, J. (2006). Investigating landslides with space-borne SAR interferometry. *Engineering Geology, 88*, 173–199.

Ferretti, A., Prati, C., & Rocca, F. (2001). Permanent scatterers in SAR interferometry. *IEEE Transactions on Geoscience and Remote Sensing, 39*(1), 8–20.

Ghilani, C. D., & Wolf, P. R. (2012). *Elementary Surveying: An Introduction to Geomatics*. Prentice Hall, Pearson, pp. 983.

Grieves, M., & Vickers, J. (2017). Digital Twin: Mitigating Unpredictable, Undesirable Emergent Behavior in Complex Systems. In: Kahlen, J., Flumerfelt, S., Alves, A. (eds) *Transdisciplinary Perspectives on Complex Systems*. Springer, Cham. https://doi.org/10.1007/978-3-319-38756-7_4

Hammer, Ø., Harper, D. A. T., & Ryan, P. D. (2001). PAST: Paleontological Statistics software package for education and data analysis. *Palaeontologia Electronica, 2001, 4*(1), 1–9.

Hoek, E., & Brown, E. T. (1980). Underground excavations in rock. CRC Press, London, pp. 536.

Jing, L. (2003). A review of techniques, advances and outstanding issues in numerical modelling for rock mechanics and rock engineering. *International Journal of Rock Mechanics and Mining Sciences, 40*, 283–353.

Jolliffe, I. T. (2002). *Principal Component Analysis*. Springer, pp. 488.

Kaufman, L., & Rousseeuw, P. J. (1990). *Finding Groups in Data: An Introduction to Cluster Analysis.* John Wiley, Hoboken. http://dx.doi.org/10.1002/9780470316801.ch1

Leica Geosystems, A. G. (2025a). Leica RTC360 3D Reality Capture Solution. 2025. Available online: https://leica-geosystems.com/products/laser-scanners/scanners/leica-rtc360 (accessed on 31 July 2025).

Leica Geosystems, A. G. (2025b). Leica Infinity Surveying Software. 2025. Available online: https://leica-geosystems.com/en-us/products/gnss-systems/software/leica-infinity

Lindenbergh, R., & Pfeifer, N. (2005). A statistical deformation analysis of two epochs of terrestrial laser data. *ISPRS Journal of Photogrammetry and Remote Sensing, 61*, 119–134.

Marina, O. (2023). *Monitorizarea şi analiza deplasărilor terenului de la zi şi a planşeelor dintre etaje aflate sub influenţa exploatării subterane a zăcământului de sare de la Slănic-Prahova* [Monitoring and analysis of surface ground movements and interlevel floor displacements under the influence of underground mining at the Slănic-Prahova salt deposit] [Doctoral dissertation, University of Petroşani].

Massonnet, D., & Feigl, K. L. (1998). Radar interferometry and its application to changes in the Earth's surface. *Reviews of Geophysics, 36*(4), 441–500.

Munson, D. E., & Dawson, P. R. (1979). *Constitutive model for the low temperature creep of salt (with application to WIPP)*. Sandia National Laboratories, Report SAND79-1853.

Naumowicz, B., & Kowalczyk, K. (2025). Integration of leveling and GNSS data to develop relative vertical movements of the Earth's crust using hybrid models. *Applied Sciences, 15*(15), 8224.

Oprina, C. A. (2015), *Posibilităţii de exploatare a zăcămintelor de sare gema situate la adâncimi mari*, [Possibilities for the exploitation of rock salt deposits located at great depths] [Doctoral dissertation, University of Petroşani].

Săndulescu, M. (1984). *Geotectonica României* [Geotectonics of Romania] Editura Tehnică, Bucuresti, pp 336.

Sîrbu, O. M., Vîlceanu, C. -B., Moscovici, A. M., & Herban, S. (2022). Open-source GIS for territorial planning - Solar map of Timiş County, Romania. *Scientific Papers. Series E. Land Reclamation, Earth Observation & Surveying, Environmental Engineering, XI*, 444–451.

Sîrbu, O. M., Vîlceanu, C. -B., Moscovici, A. M., ILIESCU, A. -I., CHENDEŞ, R., & Anderca, O. -M. (2023). Monitoring of "Dealul Maria" marble perimeter, Ruschiţa, Caraş-Severin County. *Scientific Papers. Series E. Land Reclamation, Earth Observation & Surveying, Environmental Engineering, XII*, 11–18.

Tereşneu, C. C., & Tereşneu, C. S. (2023). GIS facilities for the automation of cadastral documentations. *Scientific Papers. Series E. Land Reclamation, Earth Observation & Surveying, Environmental Engineering, XII*, 371–376.

Teunissen, P. J. G., & Kleusberg, A. (1998). *GPS for Geodesy*. Springer Berlin Heidelberg, pp. 650. https://doi.org/10.1007/978-3-642-72011-6

Vosselman, G., & Maas, H. G. (2010). *Airborne and Terrestrial Laser Scanning.* CRC Press, pp. 320.

Wolfram Research, Inc., Mathematica, Version 14.2, Champaign, IL (2024).